Graph theory, geometric probabilities, and a representative width for three-dimensional detonation cells

Vianney Monnier, Pierre Vidal, Vincent Rodriguez, Ratiba Zitoun
Institut Pprime, UPR 3346 CNRS, ENSMA, BP 40109, 86961 Futuroscope-Chasseneuil, France

1. Introduction

First identified experimentally in the late 1950s [1], the cellular structure of the detonation reaction zone in gases is viewed today as an example of non-linear instability of combustion waves in compressible reactive fluids, e.g. [2, 3, 4]. It is now recognized that physical representations of this unsteady structure can only be three-dimensional. Experimental and numerical analyses of front views of detonation waves, e.g. [5, 6], evidence that the cellular structure is made up of irregular patterns if the number of cells on the front surface is sufficiently large. That is typically observed in the case of detonation propagation in tubes with cross sections sufficiently large because the usual cell descriptor, namely its mean width $\overline{\lambda}$, decreases when increasing the initial pressure p_0 of the gas. The accepted modelling framework then involves hydrodynamics and chemical kinetics solely and no significant participation of viscosity, for example, from boundary layers and turbulence. A topic of debate is whether a unique characteristic length is relevant to characterizing a 3D cell. The model below assumes that such is the mean width $\overline{\lambda}$ and, therefore, elaborates on the analysis outlined from our recordings of three-dimensional detonation cells [5] and presented to the 28th ICDERS (Naples 2022, paper #57).

The three ingredients are graph theory, geometric probabilities and the Zel'dovich-Von Neuman-Döring (ZND) model of planar detonation. First (Sect.2), we express the physical premise that the 3D unsteady cellular process for irregular cells is stochastic and should produce the same burnt mass as the average planar steady ZND process per unit of time. Then (Sect.3), we use graph theory to define an ideal cell whose grouping is equivalent to the real 3D cellular front [5] and geometric probabilities to determine the mean burnt fraction that parameterizes the model. Finally (Sect.4), we implement the ZND model with detailed schemes of chemical kinetics to calculate the relation time-position of a fluid element in the ZND steady reaction zone, respective to its leading shock, which closes the problem of determining $\overline{\lambda}$. The comparison of measured and calculated $\overline{\lambda}$ shows agreement to better than or within the accepted experimental uncertainties, depending on the reactive mixture, its initial pressure p_0 and equivalence ratio. Thus, the quality of this estimate is dependent solely on that of the chemical kinetics scheme, the modelling assumptions aside. The model is readily implementable as a post-process of ZND profiles that provides instantaneously the estimates of the cell width, length and reaction time, as well as the ZND reaction length and time.

2. Model

The basic assumption is that the cellular and ZND processes burn the fresh mixture at the same mass rate for sufficiently large periods and the same projected front area. Let t and z denote the time and the position in the ZND reaction zone, respective to its leading shock, and Δt_{C} the period during which the ZND front travels the distance L_{C} representing the length of the ideal cell. For the self-sustained detonation propagating at the Chapman-Jouguet (CJ) velocity D_{CJ},

$$L_{\mathrm{C}} = D_{\mathrm{CJ}} \Delta t_{\mathrm{C}}. \tag{1}$$

A reaction time below refers to the period necessary to completely burn all fluid elements captured by a front at the initial instant $t = 0$ and through the same reference surface area. Thus, in the ZND process, denoting by t_{Z} its reaction time, the fluid elements entered in the reaction zone during the period $0 < t \leqslant t_{\mathrm{Z}}$ can only be partially burnt at t_{Z}. That results in the mean ZND burnt fraction $\overline{y}_{\mathrm{Z}}$ and reaction rate $\overline{y}_{\mathrm{Z}}/t_{\mathrm{Z}}$. In the cellular process, the front is a grouping of forward-convex waves whose forefront velocities for irregular

Correspondence to: pierre.vidal@ensma.fr

cells randomly vary about the ZND mean velocity, such as D_{CJ}. Their boundaries are the intersections with transverse waves that sweep the surfaces of the forward waves with lower velocities. High-speed recordings, e.g. [7, 8, 9] indicate that combustion is ensured at an instantaneous rate much rapid in the domains behind the transverse waves and the forward waves with higher velocities, that is, much faster than the mean cellular rate. A symmetry argument then suggests that the reaction time, as defined above, of the ideal cell should be half the cell time $\Delta t_{\mathrm{C}}/2$. Indeed, the period $[0, \Delta t_{\mathrm{C}}/2]$ is that necessary, on average, for the transverse waves to sweep a projected front area equivalent to the maximum area of the ideal cell, which, by symmetry, occurs every cell half length $L_{\mathrm{C}}/2$. Thus, during this period, they cover the surface of the ideal cell, and they can capture and burn all the fluid elements that have crossed the lower-velocity front surfaces since $t = 0$. That results in the mean cell burnt fraction $\bar{y}_{\mathrm{C}}$ and reaction rate $2/\Delta t_{\mathrm{C}}$–and not $\bar{y}_{\mathrm{C}} \times 2/\Delta t_{\mathrm{C}}$. These means of the mass fractions y_{Z} and y_{C} are relative to periods elapsed since $t = 0$. They write

$$\bar{y}_{\mathrm{Z}} = \frac{1}{t_{\mathrm{Z}}} \int_0^{t_{\mathrm{Z}}} y_{\mathrm{Z}}(t')dt', \quad \bar{y}_{\mathrm{C}} = \frac{2}{\Delta t_{\mathrm{C}}} \int_0^{\Delta t_{\mathrm{C}}/2} y_{\mathrm{C}}(t')dt', \tag{2}$$

where the subscripts Z and C denote the ZND and the cellular processes. The first definition above also applies to any variable, for example, the material speed $U_{\mathrm{Z}}(t) = dz(t)/dt$ at the time t, or the position $z(t)$ of a fluid element, in the ZND reaction zone. This defines the ZND reaction length ℓ_{Z} by

$$\ell_{\mathrm{Z}} = \int_0^{t_{\mathrm{Z}}} U_{\mathrm{Z}}(t')dt' = \bar{U}_{\mathrm{Z}} \times t_{\mathrm{Z}}, \quad \bar{U}_{\mathrm{Z}} = \frac{\ell_{\mathrm{Z}}}{t_{\mathrm{Z}}}, \tag{3}$$

where $\bar{U}_{\mathrm{Z}}$ denotes the mean of $U_{\mathrm{Z}}(t)$. With v denoting the specific volume, and v_0 its initial value, the relation of mass conservation written as $v_{\mathrm{Z}}(t) D_{\mathrm{CJ}} = v_0 U_{\mathrm{Z}}(t)$ at the position $z(t)$ can also be averaged, so (3) rewrites

$$\ell_{\mathrm{Z}} = \frac{\bar{v}_{\mathrm{Z}}}{v_0} D_{\mathrm{CJ}} \times t_{\mathrm{Z}}, \tag{4}$$

$$\bar{v}_{\mathrm{Z}}(\bar{y}_{\mathrm{Z}}) = (1 - \bar{y}_{\mathrm{Z}})\, v_{\mathrm{H}} + \bar{y}_{\mathrm{Z}} v_{\mathrm{CJ}}. \tag{5}$$

Relation (5) results from the averaging of the volume additivity constraint $v = \sum y_i v_i$, where v_i and y_i denote the specific volume and the mass fraction of the chemical species i, and v_{H} and v_{CJ} the specific volumes at the ZND shock and reaction end positions.

The equality of the mean reaction rates of the cellular and ZND processes implies that of their mean reaction progress variables $\bar{y}_{\mathrm{C}}$ and $\bar{y}_{\mathrm{Z}}$ respective to their reaction times $\Delta t_{\mathrm{C}}/2$ and t_{Z}, so

$$\frac{2}{\Delta t_{\mathrm{C}}} = \frac{\bar{y}}{t_{\mathrm{Z}}}, \tag{6}$$

where $\bar{y}$ denotes $\bar{y}_{\mathrm{C}} = \bar{y}_{\mathrm{Z}}$. The combination of (1) with (6) gives the relation (7) between the cell length L_{C} and the ZND reaction time t_{Z}, which, with (4) and (5), gives the relation (8) between L_{C} and the ZND reaction length ℓ_{Z}, that is,

$$L_{\mathrm{C1}}(\bar{y}, t_{\mathrm{Z}}) = k_1 \times t_{\mathrm{Z}}, \quad k_1(\bar{y}) = \frac{2}{\bar{y}} D_{\mathrm{CJ}}, \tag{7}$$

$$L_{\mathrm{C2}}(\bar{y}, \ell_{\mathrm{Z}}) = k_2 \times \ell_{\mathrm{Z}}, \quad k_2(\bar{y}) = \frac{2}{\bar{y}} \frac{v_0}{\bar{v}_{\mathrm{Z}}(\bar{y})}. \tag{8}$$

In the next section, graph theory is used to define a cellular pattern statistically equivalent to those on an irregular 3D cellular front, hence the ideal cell to which geometric probabilities are applied to obtain $\bar{y}$. The cell length L_{C} is defined by the intersection of the curves $L_{\mathrm{C1}}(t) = k_1 \times t$ and $L_{\mathrm{C2}}(t) = k_2 \times z(t)$, with the relation time-position $z(t)$ of a fluid element preliminary determined through classical ZND numerical calculations with a detailed scheme of chemical kinetics. The ZND reaction time t_{Z} and length ℓ_{Z} are then obtained from (7) and (8), and, finally, the cell width $\bar{\lambda}$ is geometrically related to L_{C}.

3. Graph theory and geometric probabilities

In our preliminary analysis [5], we considered the front-view distribution of the same pattern, for example, rectangle, pentagon, hexagon, etc., to be statistically independent of the front position if the cell number F, that is the initial pressure p_0, is sufficiently large. Indeed, several experiments carried out in the same conditions should return the same distribution. We used elements from planar graph theory to show that these irregular front views are equivalent to tessellations of hexagons. This was obtained by combining the physical condition that only three transverse waves can intersect with the mathematical limit at large F of the Descartes-Euler-Poincaré relation $F-E+V=2$ that connects the numbers of faces F (the cells), edges E (the transverse waves) and vertices V (the edge intersections) in a tessellation. For three-edge vertices, $2E=3V$, so the limit at large F of the edge number per face $2E/F$ is 6. One consequence is that a cell counting on an experimental recording gives an estimate of the cell mean width through

$$\bar{\lambda}=\frac{3\ln 3}{\pi}\frac{\sqrt{3}}{2}d_{\mathrm{x}},\quad d_{\mathrm{x}}=\sqrt{\frac{8}{3\sqrt{3}}A_{\mathrm{C}}},\quad A_{\mathrm{C}}=\frac{A_{\mathrm{T}}}{F}, \tag{9}$$

where d_{x} and A_{C} are the outer diameter and the area of the hexagon, and A_{T} the cross-section area of the tube. Another consequence, detailed below, is that a combination of properties of this representative tessellation and geometric probabilities predicts the mean reaction progress variable $\bar{y}$ and hence the cell mean width $\bar{\lambda}$ (Sect.2). The premise is that the motion of the transverse waves for irregular cells is stochastic.

First, we define a control volume with the surface area A_{C} and the half length $L_{\mathrm{C}}/2$ of the ideal cell. We denote by M_{C} the mass contained in this volume, $M\left(t\right)$ the mass having crossed the area A_{C} since $t=0$ at the intermediate instant $0<t\leqslant\Delta t_{\mathrm{C}}/2$ (or the front position $0<x\left(t\right)\leqslant L_{\mathrm{C}}/2$ in the laboratory frame), and $M_{\mathrm{B}}\left(t\right)$ the mass burnt at this instant t. They write

$$M_{\mathrm{C}}=\rho_0 A_{\mathrm{C}}\times\frac{L_{\mathrm{C}}}{2},\quad M\left(t\right)=\rho_0 A_{\mathrm{C}}\times x\left(t\right),\quad M_{\mathrm{B}}\left(t\right)=\rho_0 A_{\mathrm{B}}\left(t\right)\times x\left(t\right), \tag{10}$$

where ρ_0 denotes the initial specific mass and $A_{\mathrm{B}}\left(t\right)$ the surface area swept by the transverse waves at the instant t since $t=0$. Thus, the burnt mass fraction y_{C} at the instant t is

$$y_{\mathrm{C}}\left(t\right)=\frac{M_{\mathrm{B}}\left(t\right)}{M\left(t\right)}=\frac{A_{\mathrm{B}}\left(t\right)}{A_{\mathrm{C}}}, \tag{11}$$

so its mean $\bar{y}_{\mathrm{C}}$ (2) is the mean combustion area respective to the cell area A_{C}.

Next, we express the stochasticity of the transverse-wave motion. The successive positions of the transverse waves in a same experiment, projected onto the surface of the ideal cell, should be statistically equivalent to those obtained from one experiment to another at the same front position, that is, to those of line segments randomly dropped onto the surface. This ensures that combustion efficiency is, on average, independent of experiment. Thus, $\bar{y}_{\mathrm{C}}$ is the probability that the segments are completely contained in the cell surface, that is, the non-intersect probability, for the propagation period $\Delta t_{\mathrm{C}}/2$. The calculation is a classical problem of geometric probabilities, namely the Buffon's needle problem extended to a surface with a hexagonal tiling and needle lengths varying between 0 and the hexagon outer diameter d_{x}. In the many accounts of such problems, the non-intersection probabilities are expressed as a ratio μ_{C}/μ, where μ is the measure of the space of the independent variables representing all the random orientations and positions of a segment, and μ_{C} the measure of the subspace in which these variables should vary so the segments do not intersect the boundaries of the typical tessellation element. For the hexagon, we extend below to a variable-length segment the solution by Vassallo [10] for a constant-length segment. We do not reproduce his calculations for conciseness and because of the clarity of his account. The independent variables are the segment length s varying in $[0,d_{\mathrm{x}}]$, its angle θ varying in $[0,2\pi]$, and the coordinates of its center varying in the cell surface of area A_{C}. The non-intersection constraint demands this center to be contained into a smaller surface than that of the cell, and whose shape and area depend on the segment orientation and length. Nondimensionalizing the lengths by the side length $d_{\mathrm{x}}/2$ of the typical hexagon, and denoting by

$r = 2s/d_{\rm x}$ the non-dimensional segment lengths, we have

$$\mu = 6\pi\sqrt{3}, \quad \mu_{\rm C} = m_1 + m_2 + m_3, \quad m_i = \int_{r_{i1}}^{r_{i2}} \mu_i\,(r)\,dr, \tag{12}$$

$$r \in [r_{11} = 0, r_{12} = 1]\,, \quad \mu_1\,(r) = 3\pi\sqrt{3} - 12r + r^2\left(3 - \pi/\sqrt{3}\right), \tag{13}$$

$$r \in \left[r_{21} = 1, r_{22} = \sqrt{3}\right], \quad \mu_2\,(r) = \pi\sqrt{3}\left(r^2 + 5\right) - 9\sqrt{4r^2 - 3}\ ... \tag{14}$$

$$... \ - 2\sqrt{3}\left(3 + 2r^2\right)\arcsin\left(\sqrt{3}/2r\right), \tag{15}$$

$$r \in \left[r_{31} = \sqrt{3}, r_{32} = 2\right], \quad \mu_3\,(r) = 2\sqrt{3}\left(r^2 + 12\right)\arcsin\left(\sqrt{3}/r\right)\ ... \tag{16}$$

$$... \ + 30\sqrt{r^2 - 3} - \left(8\pi\sqrt{3} + 18\right) - r^2\left(3 + 2\pi/\sqrt{3}\right), \tag{17}$$

$$m_1 = 10.720, \quad m_2 = 1.837\,4, \quad m_3 = 1.154\,7 \times 10^{-2}, \tag{18}$$

where the μ_is are Vassallo's non-intersection measures for constant segment lengths [10] and the m_is ours for segment lengths varying in the intervals $[0, d_{\rm x}/2]$, $\left[d_{\rm x}/2, \sqrt{3}d_{\rm x}/2\right]$ and $\left[\sqrt{3}d_{\rm x}/2, d_{\rm x}\right]$. This gives the non-intersection probability, that is, the mean burnt fraction $\bar{y}_{\rm C}$ ($\equiv \bar{y}$, Sect.2), by

$$\mu = 32.648, \quad \mu_{\rm C} = 12.569, \quad \bar{y} = \frac{\mu_{\rm C}}{\mu} \approx 0.38498, \tag{19}$$

so, from (6), the cellular process takes, on average, $\Delta t_{\rm C}/t_{\rm Z} \approx 5.2$ times longer than the ZND process to achieve combustion.

Finally, we obtain the aspect ratio $\bar{\lambda}/L_{\rm C}$ by combining stochasticity and, inspired by [11], geometry. Since the transverse waves have a stochastic motion, their positions can be considered to be the same every period $\Delta t_{\rm C}$, so the longitudinal overdriven front waves of the model cellular front should superimpose on each other every distance $L_{\rm C}$. Equivalently, these waves can be viewed as the upper surface elements of spheres arranged in the hexagonal closest packing, that is, with alternate layers in the ABAB ... sequence. The sphere diameter is also the distance between the centers of adjacent spheres and the inner diameter of a hexagon, $d_{\rm i}$, so the ratio $L_{\rm C}/d_{\rm i}$ comes out as twice the height of the tetrahedral pyramid whose base is the triangle with vertices the centers of the three closest spheres in the same layer. Simple geometry then gives $L_{\rm C}/d_{\rm i} = \sqrt{8/3}$ and $d_{\rm i}/d_{\rm x} = \sqrt{3}/2$. With the first relation (9), that yields the mean cell aspect ratio

$$\frac{\bar{\lambda}}{L_{\rm C}} = \frac{3\ln 3}{\pi}\sqrt{\frac{3}{8}} \approx 0.64244 \tag{20}$$

and opening angle 65.4° well representing the measurements on longitudinal recordings and, with (6), (19) and the basic relation between mass and volume fractions, the ratio of lengths $L_{\rm C}/\ell_{\rm Z}$ and $\bar{\lambda}/\ell_{\rm Z}$ which take the accepted large values of $\approx 20 - 40$, depending on $v_{\rm H}$ and $v_{\rm CJ}$.

4. Results and discussion

For conciseness, we do not detail in this abstract the classical system of 1st order ordinary differential equations that governs the ZND model. The quality of the chemical kinetics schemes implemented in the ZND calculations determines that of the cell mean width estimates by the model above, its assumptions aside. We selected mixtures with H_2, C_3H_8 or CH_4 as the fuel and O_2 or Air as the oxidizer because of their practical importance and the attention they have received from kineticists, and we thus used the Konnov [12] and the FFCM-1 [13] detailed schemes.

Figure 1 compares the calculation results (full and open symbols ◆, ◇, ▲) to measurements in tubes (crosses) as presented in the detonation database [14]. Denoting by d the transverse dimensions of the tubes, the black (+) and grey (×) crosses denote values of the ratio $\bar{\lambda}/d$ smaller and larger, respectively, than the arbitrary magnitude $\mathcal{O}(10)$. That gives $\mathcal{O}(100)$ cells on the front surface, which we considered to be a number sufficiently large to meet the model's basic assumption. We collected the tube dimensions from the original references.

The comparison shows a very good agreement by the trends and the magnitudes and, in most cases, to better than the $\approx 50 - 100\%$ typical standard deviation for the mean width of irregular cells. Overall, the smaller the cell mean width compared to the tube dimension, i.e., the black crosses +, the better the agreement, consistent with the assumption of many cells on the front surface. The agreement is also better with mixture compositions close to the stoichiometric balance, perhaps because this is the usual calibration range of kinetic schemes.

The cell mean width is still considered to be a useful characteristic length in detonation dynamics, although the complex 3D patterns observed on detonation front views question the sufficiency of its representativeness and are the likely reason for the large standard deviations. In view of this intrinsic limitation, we felt that simple global modelling could yield a representative cell width sufficiently accurate for practical purposes without detailing the complex wave interactions that form the cellular structure.

Our approach does not pretend to explain how the detonation reaction zones are unstable and only assumes a global equivalence of the ZND and cellular processes expressed by basic conservation and action principles. Since its implementation is an easy post-process of ZND profiles, a complementary application is its use as an inverse method to assess the representative capacity of kinetic schemes from cell measurements obtained in conditions that eliminate the confinement effects. Current work includes a better representation of the cellular front using a Voronoi tessellation with a statistical distribution of several patterns, other mixtures and schemes–we obtained the same good agreement with the San-Diego mechanism, where applicable–and a comparative discussion with regular cells, which we hope to also present to the Colloquium.

References

[1] Y. N. Denisov, Y. K. Troshin, Pulsating and spinning detonation of gaseous mixtures in tubes. Dokl. Akad. Nauk SSSR, 125(1) (1959) 110-113, and also: Structure of gaseous detonation in tubes. Sov. Phys. Tech. Phys., 5(4) (1960) 419-431

[2] M. Short, G.J. Sharpe, Pulsating instability of detonations with a two-step chain-branching reaction model: theory and numerics, Combust. Theor. Model. 7 (2) (2003) 401–416 | doi:10.1088/1364-7830/7/2/311

[3] M. Radulescu, G.J. Sharpe, D. Bradley, A universal parameter quantifying explosion hazards, detonability and hot spot formation: χ number, in: D. Bradley et al. (Eds.), Proc. Int. Seminar on Fire and Explosion Hazards, Research Publishing, 2013, 617–626 | doi:10.3850/978-981-07-5936-0_10-01

[4] P. Clavin, G. Searby, Combustion Waves and Fronts in Flows: Flames, Shocks, Detonations. Ablation Fronts and Explosion of Stars, Cambridge University Press (2016) | doi:10.1017/CBO9781316162453

[5] V. Monnier, V. Rodriguez, P. Vidal, R. Zitoun, An analysis of three-dimensional patterns of experimental detonation cells, Combustion and Flame, 245 (2022) 112310 | doi:10.1016/j.combustflame.2022.112310

[6] J. Crane, J.T. Lipkowicz, X. Shi, I. Wlokas, A.M. Kempf, H. Wang, Three-dimensional detonation structure and its response to confinement, Proc. Combustion Inst. (2022) | doi:10.1016/j.proci.2022.10.019

[7] F. Pintgen, J. E. Shepherd, Simultaneous Soot Foil and PLIF Imaging of Propagating Detonations, Proc. 19$^{\text{th}}$ ICDERS (2003) Paper 119

[8] F. Pintgen, C.A. Eckett, J.M. Austin, J.E. Shepherd, Direct observations of reaction zone structure in propagating detonations, Combustion and Flame, 133(3) (2003) 211-229 | doi:10.1016/S0010-2180(02)00458-3

[9] J.M. Austin, F. Pintgen, J.E. Shepherd, Reaction zones in highly unstable detonations, Proc. Combustion Inst., (2005) 1849–1857 | doi:10.1016/j.proci.2004.08.157

[10] S.F. Vassallo, Buffon's coin and needle problems for the snub hexagonal tiling, Advances in Mathematics: Scientific Journal, 10 (4) (2021) 2223-2233 | doi:10.37418/amsj.10.4.36

[11] R. Takai, K. Yoneda, T. Hikita, Study of detonation wave structure, Proc. Combustion Inst. 15(1) (1975), 69-78 | doi:10.1016/S0082-0784(75)80285-2

[12] F.H.V. Coppens, J. De Ruyck, A.A. Konnov, The effects of composition on burning velocity and nitric oxide formation in laminar premixed flames of $CH_4 + H_2 + O_2 + N_2$, Combustion and Flame, 149(4) (2007) 409-417 | doi:10.1016/j.combustflame.2007.02.004

[13] G.P. Smith, Y. Tao, H. Wang, Foundational Fuel Chemistry Model Version 1.0 (FFCM-1) 2016 | http://nanoenergy.stanford.edu/ffcm1

[14] M. Kaneshige, J.E. Shepherd, Detonation database. Technical Report FM97-8, GALCIT, July 1997 | http://www.galcit.caltech.edu

Figures

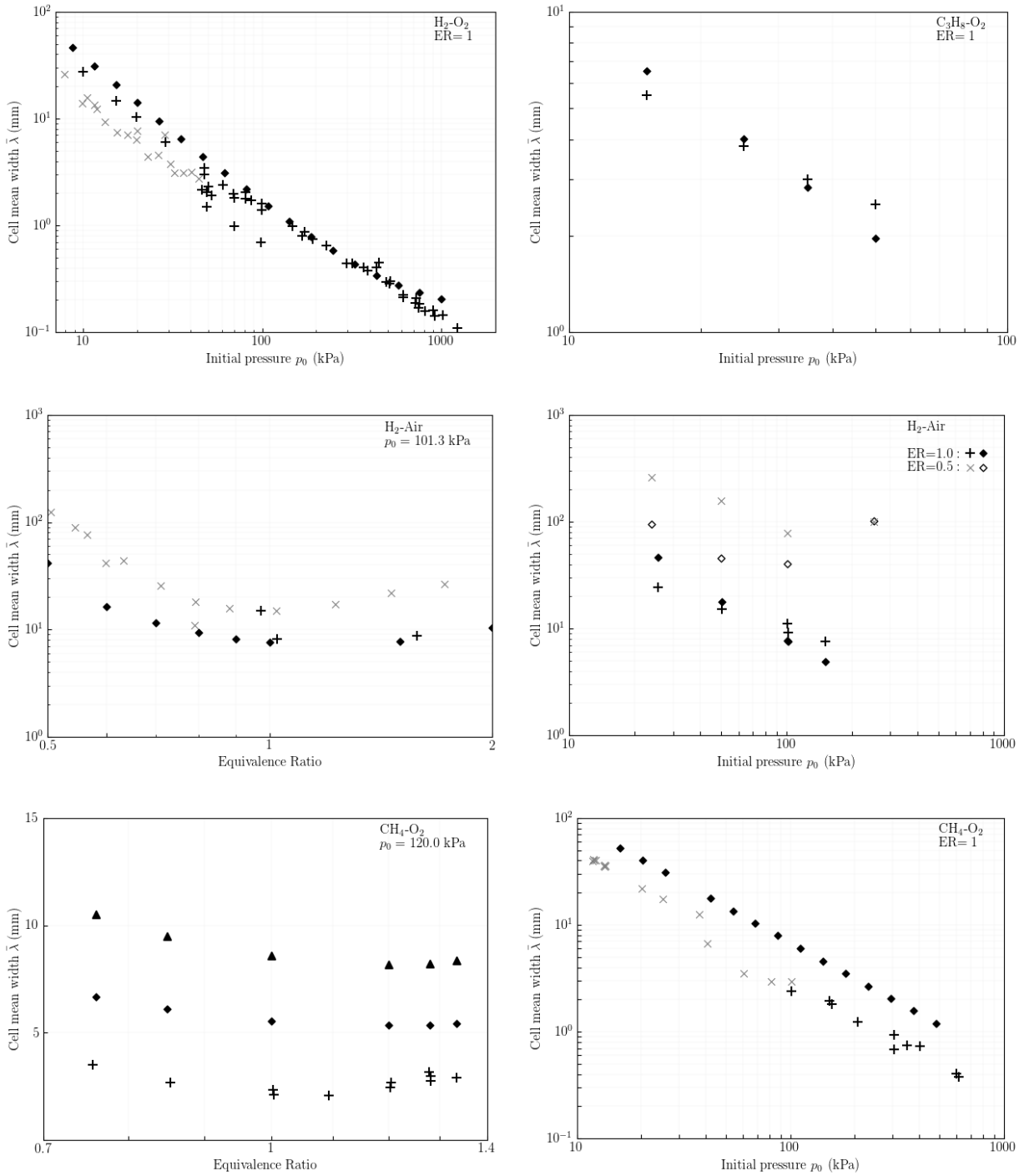

Figure 1: Comparison of calculated and measured cell mean widths $\bar{\lambda}$. Full and open symbols: calculations using the Konnov [12] (◆ and ◇) and the FFCM-1 [13] (▲) schemes of chemical kinetics. Crosses: measurements [14] with small ($\leqslant \mathcal{O}(10)$, black +) and large ($\geqslant \mathcal{O}(10)$, grey ×) ratios $\bar{\lambda}/d$, with d the transverse dimensions of the tubes.